Magnetic dipole super-resonances and their impact on mechanical forces at optical frequencies

Iñigo Liberal,[1] **Iñigo Ederra,**[1] **Ramón Gonzalo,**[1] **and Richard W. Ziolkowski**[2*]

[1] *Antenna Group, Public University of Navarra, Pamplona, 31006 Spain*

[2] *Department of Electrical and Computer Engineering, University of Arizona, Tucson, AZ, 85721 USA*

** ziolkowski@ece.arizona.edu*

Abstract: Artificial magnetism enables various transformative optical phenomena, including negative refraction, Fano resonances, and unconventional nanoantennas, beamshapers, polarization transformers and perfect absorbers, and enriches the collection of electromagnetic field control mechanisms at optical frequencies. We demonstrate that it is possible to excite a magnetic dipole super-resonance at optical frequencies by coating a silicon nanoparticle with a shell impregnated with active material. The resulting response is several orders of magnitude stronger than that generated by bare silicon nanoparticles and is comparable to electric dipole super-resonances excited in spaser-based nanolasers. Furthermore, this configuration enables an exceptional control over the optical forces exerted on the nanoparticle. It expedites huge pushing or pulling actions, as well as a total suppression of the force in both far-field and near-field scenarios. These effects empower advanced paradigms in electromagnetic manipulation and microscopy.

OCIS codes: (160.3918) Metamaterials; (250.5403) Plasmonics; (290.4020) Mie theory; (290.0290) Scattering.

References and links

1. L. D. Landau and E. M. Lifshitz, *Electrodynamics of Continuous Media* (Pergamon, 1960).
2. R. Merlin, "Metamaterials and the Landau-Lifshitz permeability argument: large permittivity begets high-frequency magnetism," Proc. Natl Acad. Sci. USA **106**, 1693-1698 (2009).
3. V. M. Shalaev, "Optical negative-index metamaterials," Nat. Photon. **1**, 41-48 (2007).
4. N. Liu, L. Fu, S. Kaiser, H. Schweizer and H. Giessen, "Plasmonic building blocks for magnetic molecules in three-dimensional optical metamaterials," Adv. Mater. **20**, 3859-3865 (2008).
5. H.-K. Yuan, U. K. Chettiar, W. Cai, A. V. Kildishev, A. Boltasseva, V. P. Drachev, and V. M. Shalaev, "A negative permeability material at red light," Opt. Express **15**, 1076-1083 (2007).
6. A. Alù and N. Engheta, "The quest for magnetic plasmons at optical frequencies," Opt. Express **17**, 5723-5730 (2009).
7. U. Leonhardt, "Optical conformal mapping," Science **312**, 1777-1780 (2006).
8. J. B. Pendry, D. Schurig, and D. R. Smith, "Controlling electromagnetic fields," Science **312**, 1780-1782 (2006).
9. J. B. Pendry, "Negative refraction makes a perfect lens," Phys. Rev. Lett. **85**, 3966-3969 (2000).
10. M. Kerker, D. S. Wang, and C. L. Giles, "Electromagnetic scattering by magnetic spheres," J. Opt. Soc. Am. A **73**, 765-767 (1983).
11. Y. H. Fu, A. I. Kuznetsov, A. E. Miroshnichenko, Y. F. Yu, and B. Lukyanchuk, "Directional visible light scattering by silicon nanoparticles," Nature Commun. **4**, 1527 (2013).

12. S. Person, M. Jain, Z. Lapin, J. J. Sáenz, G. Wicks, and L. Novotny "Demonstration of zero optical backscattering from single nanoparticles," Nano Lett. **13**, 1806-1809 (2013).
13. S. D. Campbell, and R. W. Ziolkowski, "Simultaneous excitation of electric and magnetic dipole modes in a resonant core-shell particle at infrared frequencies to achieve minimal backscattering," J. Select. Topics Quantum Electronics **19**, 4700209 (2013).
14. F. Shafiei, F. Monticone, K. Q. Le, X.-X. Liu, T. Hartsfield, A. Alù and X. Li, "A subwavelength plasmonic metamolecule exhibiting magnetic-based optical Fano resonance," Nature Nanotech. **8**, 95-99 (2013).
15. S. N. Sheikholeslami, A. García-Etxarri, , and J. A. Dionne, "Controlling the interplay of electric and magnetic modes via Fano-like plasmon resonances," Nano Lett. **11**, 3927-3934 (2011).
16. C. Pfeiffer, and A. Grbic, "Metamaterial Huygens surfaces: tailoring wave fronts with reflectionless sheets," Phys. Rev. Lett. **110**, 7401-7405 (2013).
17. T. Niemi, A. O. Karilainen, and S. A.Tretyakov, "Synthesis of polarization transformers," IEEE Trans. Antennas Propag. **61**, 3102-3111 (2013).
18. Y. Ra'di, V. S. Asadchy, and S. A. Tretyakov, "Total absorption of electromagnetic waves in ultimately thin layers," IEEE Trans. Antennas Propag. **61**, 4606-4614 (2013).
19. A. García-Etxarri, R. Gómez-Medina, L. S. Froufe-Pérez, C. López, L. Chantada, F. Scheffold, J. Aizpurua, M. Nieto-Vesperinas, and J. J. Sáenz, "Strong magnetic response of submicron silicon particles in the infrared," Opt. Express **19**, 4815-4826 (2011).
20. H. H. Li, "Refractive index of silicon and germanium and its wavelength and temperature derivatives," J. Phys. Chem. Ref. Data **9**, 561 (1980).
21. A. I. Kuznetsov, A. E. Miroshnichenko, Y. H. Fu, J. Zhang, and B. Lukyanchuk, "Magnetic light," Nature Sci. Reports **2**, 492 (2012).
22. A. B. Evlyukhin, S. M. Novikov, U. Zywietz, R. L. Eriksen, C. Reinhardt, S. I. Bozhevolnyi,and B. N. Chichkov, "Demonstration of magnetic dipole resonances of dielectric nanospheres in the visible region," Nano Lett.**12**, 3749-3755 (2012).
23. J. A. Gordon and R. W. Ziolkowski, "The design and simulated performance of a coated nano-particle laser," Opt. Express **15**, 2622-2653 (2007).
24. M. A. Noginov, G. Zhu, A. M. Belgrave, R. Bakker, V. M. Shalaev, E. E. Narimanov, S. Stout, E. Herz, T. Suteewong, and U. Wiesner,"Demonstration of a spaser-based nanolaser. Nature Photon. **460**, 1110-1113 (2009).
25. N. I. Zheludev, S. L. Prosvirnin, N. Papasimakis, and V. A. Fedotov, "Lasing spaser," Nature Photon. **2**, 351-354 (2008).
26. S. Arslanagić and R. W. Ziolkowski, "Active coated nano-particle excited by an arbitrarily located electric Hertzian dipoleresonance and transparency effects" J. Opt. **12**, 024014 (2010).
27. P. C. Chaumet, and A. Rahmani, "Electromagnetic force and torque on magnetic and negative-index scatterers," Opt. Express **17**, 2224-2234 (2009).
28. M. Nieto-Vesperinas, J. J. Sáenz, R. Gómez-Medina, and L. Chantada, "Optical forces on small magnetodielectric particles," Opt. Express **18**, 428-443 (2010).
29. M. Nieto-Vesperinas, R. Gómez-Medina, and J. J. Sáenz, "Angle-suppressed scattering and optical forces on submicrometer dielectric particles," J. Opt. Soc. Am. A **28**, 54-60 (2011).
30. R. Gómez-Medina, B. García-Cámara, I. Suárez-Lacalle, F. González, F. Moreno, M. Nieto-Vesperinas, and J. J. Sáenz, "Electric and magnetic dipolar response of germanium nanospheres: interference effects, scattering anisotropy, and optical forces," J. Nanophoton. **5**, 3512 (2011).
31. S. Xiao, V. P. Drachev, A. V. Kildishev, X. Ni, U. K. Chettiar, H.-K. Yuan, and V. M. Shalaev, "Loss-free and active optical negative-index metamaterials," Nature (London) **466**, 735-738 (2010).
32. N. Meinzer, M. Ruther, S. Linden, C. M. Soukoulis, G. Khitrova, J. Hendrickson, J. D. Olitsky, H. M. Gibbs, and M. Wegener, "Arrays of Ag split-ring resonators coupled to InGaAs single-quantum-well gain," Opt. Express **18**, 24140–24151 (2010).
33. N. Meinzer, M. Konig, M. Ruther, S. Linden, G. Khitrova, H. M. Gibbs, K. Busch, and M. Wegener, "Distance-dependence of the coupling between split-ring resonators and single-quantum-well gain," Appl. Phys. Lett. **99**, 111104 (2011).
34. M. Wegener, J. L. García-Pomar, C. M. Soukoulis, N. Meinzer, M. Ruther, and S. Linden, "Toy model for plasmonic metamaterial resonances coupled to two-level system gain," Opt. Express **16**, 19785–19798 (2008).
35. Sigma-Aldrich Corporation, url: http://www.sigmaaldrich.com/materials-science/nanomaterials/lumidots.html (2013).
36. S. D. Campbell, and R. W. Ziolkowski, "The performance of active coated nanoparticles based on quantum-dot gain media," Adv. OptoElectronics **36**, 8786-8791 (2012).
37. C. F. Bohren and D. R. Huffman, *Absorption and Scattering of Light by Small Particles* (Wiley, 2008).
38. P. Holmström, L. Thylén, and A. Bratkovsky, "Dielectric function of quantum dots in the strong confinement regime," J. Appl. Phys. **107**, 4307-4313 (2010).
39. I. Moreels, D. Kruschke, P. Glas, and J. W. Tomm, "The dielectric function of PbS quantum dots in a glass matrix," Opt. Mater. Express **2**, 496-500 (2012).
40. T. Kudo, and H. Ishihara, "Proposed nonlinear resonance laser technique for manipulating nanoparticles," Phys.

Rev. Lett. **109**, 7402-7406 (2012).
41. A. Mizrahi and Y. Fainman, "Negative radiation pressure on gain medium structures," Opt. Lett. **35**, 3405-3407 (2010).
42. I. Liberal, I. Ederra, R. Gonzalo, and R. W. Ziolkowski, "Near-field electromagnetic trapping through curl-spin forces," Phys. Rev. A **87**, 3807-3816 (2013).
43. S. Tricarico, F. Bilotti, and L. Vegni, "Reduction of optical forces exerted on nanoparticles covered by scattering cancellation based plasmonic cloaks," Phys. Rev. B **82**, 5109-5117 (2010).
44. R. F. Harrington, *Time-Harmonic Electromagnetic Fields* (McGraw-Hill, 1961).
45. I. Liberal, I. Ederra, R. Gonzalo, and R. W. Ziolkowski, "Electromagnetic force density in electrically and magnetically polarizable media," Phys. Rev. A **88**, 053808 (2013).
46. A. Alù, and N. Engheta, "Polarizabilities and effective parameters for collections of spherical nanoparticles formed by pairs of concentric double-negative, single-negative, and or double-positive metamaterial layers," J. Applied Phys. **97**, 094310 (2005).

1. Introduction

Because of the inherent weakness of the magnetic response of matter at optical frequencies [1, 2], there has been a great deal of excitement in the recent development of artificial magnetic properties based on metamaterial-inspired concepts [3–6]. This ability to tailor magnetic, as well as electric optical responses has facilitated the pursuit of negative refraction [3], cloaking [7, 8] and perfect lensing [9]. It has also stimulated the current investigations of Kerker-inspired Huygen's sources [10] at optical and infrared frequencies, aimed at the advancement of highly directive and efficient nanoantennas [11, 12] and the control of thermal emissions [13]. Magnetic-based Fano resonances have also attracted great interest; they feature huge field enhancements and sharp spectral features with consequent applications in the field of sensing [14, 15]. Moreover, a strong magnetic response is essential to the ultimate design of thin (one-particle thickness) beam-shapers [16], polarization transformers [17] and perfect electromagnetic absorbers [18].

As predicted theoretically [19], the relatively high refractive index of silicon (Si) $n \sim 3.5$ (see, e.g., [20]) enables the isotropic and low-loss excitation of magnetic dipole modes at optical frequencies. The existence of these magnetic resonances has been experimentally verified recently [11, 14, 21, 22]. In this article, we demonstrate that it is possible to boost the magnetic dipole resonance response of a Si nanosphere by several orders of magnitude by coating it with a shell impregnated with an active material. Moreover, although the nanoparticle retains a dominant magnetic dipolar response, this enhancement is comparable to those achieved with spaser-based nano-lasers [23–26]. Thus, this configuration attains unprecedented levels of magnetic activity at optical frequencies.

Furthermore, it is shown how that the active shell enables an exceptional control of the electromagnetically-induced mechanical forces exerted on the nanoparticle. In this regard, analytical formulations to determine the force on a particle exhibiting both electric and magnetic polarizabilities have been presented [27, 28], and numerical examples of the forces exerted by a plane wave on Si and Ge nanospheres have been reported, respectively, in [29] and [30]. Here we demonstrate that an active shell provides the degrees of freedom necessary to produce huge accelerating and/or dragging forces, as well as a complete suppression of the forces exerted on the nanoparticle in both far-field and near-field scenarios, even when it is re-radiating a significant amount of power. These force-related results empower us to envisage advanced paradigms in electromagnetic manipulation, particle sorting and microscopy.

2. Far-field analysis

A sketch of the geometry of interest is depicted in the inset of Fig. 1(a). Specifically, the nanoparticle consists of a Si nanosphere with radius $a_1 = 75\,\text{nm}$, covered by an active shell

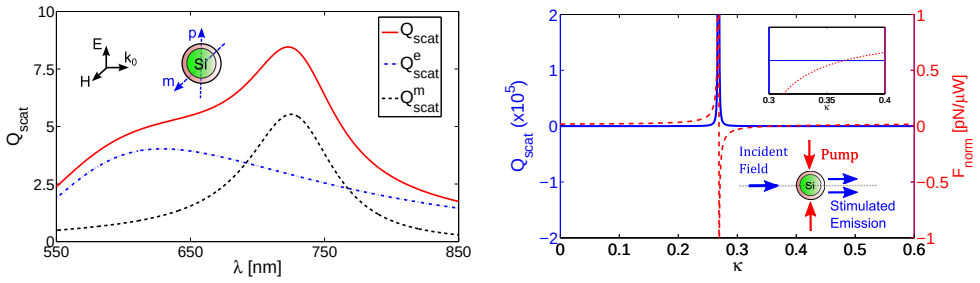

Fig. 1. (a) Scattering efficiency spectrum Q_{scat}, and the contributions to it from the electric and magnetic dipoles, Q^e_{scat} and Q^m_{scat}, respectively, for the passive case, $\kappa = 0$. Inset: Sketch of the coated Si particle illuminated by a plane-wave, and the resulting dipolar excitations. (b) Q_{scat} at the magnetic dipole resonance as a function of the imaginary part of the index of refraction, κ, as well as the mechanical force exerted on the nanoparticle, normalized to the incident electromagnetic power projected onto its physical area, $F_{\text{norm}} = F/\left(S_R \pi a_2^2\right)$. Insets: Top-right: Zero-force region. Bottom-right: Geometry.

so that its total radius is $a_2 = 120\,\text{nm}$. A number of experimental studies [31–33] have demonstrated that metamaterial structures coupled to gain media can be modeled in good agreement with Lorentzian models [34]. Therefore, as in related works that have studied active materials for nano-laser applications (e.g., [25]), the active shell will be described by a canonical model whose refractive index $n_{\text{active}} = n + j\kappa$ (corresponding to the $\exp(j\omega t)$ time-convention). Moreover, the gain values will be restricted to those attainable with commercially available core-shell CdSe/ZnS ($n \sim 2.5$) quantum-dots (QDs) [35] to demonstrate that the proposed phenomena can be achieved with realistic material parameters. Furthermore, while the dispersion properties of the gain medium itself are not considered, the coated nano-particle configuration provides a means to frequency tune its resonance to match (strongly overlap) it to the resonance of a dispersive gain medium [36].

Figure 1(a) shows the scattering efficiency Q_{scat}, defined as the total scattering cross section normalized to its cross sectional area πa_2^2 (see, e.g., [37] p. 72), for the passive case, i.e., when $\kappa = 0$. As found for bare, passive Si nanospheres [22], the Q_{scat} behavior of the core-shell configuration is dominated by the superposition of the responses arising from the electric and magnetic dipolar resonances. Figure 1(b) depicts Q_{scat} at the magnetic dipolar resonance as a function of the imaginary part of the shell refractive index, κ. In order to construct Fig. 1(b), a Q_{scat} spectrum is calculated for each κ value as in Fig. 1(a). Next, its maximum is identified and included in Fig. 1(b). Therefore, each point in Fig. 1(b) corresponds to a slightly different wavelength. Nevertheless, all of these wavelengths are located in the immediate neighborhood of 725 nm. The figure demonstrates that, although Q_{scat} monotonically increases for small κ values, there is a optimal value: $\kappa \sim 0.275$, for which a super-resonant state of the coated nanoparticle is excited and Q_{scat} is increased by several orders of magnitude. While this effect is somewhat analogous to super-resonant states excited in spaser-based nano-lasers [23–26], a collection of scattering directivity patterns, scattering efficiency spectra and field plots provided in Fig. 2 for different gain values demonstrates that the magnetic dipolar resonance is dominant at such a super-resonant state. Therefore, it can be concluded that the active coated Si nanosphere is able to provide an unprecedented magnetic response at optical frequencies. In theory, the scattering efficiency at the super-resonance is unbounded for this canonical model. In practice however, it will be limited by fabrication tolerances and the difficulty of dealing with an increasingly narrow bandwidth as the core-shell system begins to lase, as well as the

saturation of the gain media and other non-linear effects. The extent of these effects will be confined to dampening the super-resonance within a small interval of κ values centered on the super-resonance, so that the net enhancement at the super-resonance will be limited to a few of orders of magnitude as a function of the fabrication tolerances and gain medium properties.

To emphasize the field mechanism that leads to this super-resonant state, the third column of Fig. 2 gives the combined colormap and quiver (arrow) plots of the electric field at the maximum of the Q_{scat} spectrum. It can be concluded that as the particle is tuned close to the super-resonance (see Fig. 2(c)), its response is dominated by a strong circulating electric field, similar to that excited at the magnetic dipole resonance of a high-permittivity sphere [21]. The circulating field is concentrated in the outer part of the Si core and at its interface with the active shell. In this manner, and in analogy with spaser-based nano-lasers [23–26], the proposed configuration benefits from the concentration of the fields into its nanometer-sized core-shell form, which provides the feedback mechanism that leads to the super-resonance. This fact also enables the excitation of the super-resonance with realistic κ values. In particular, we note that commercially available [35] core-shell CdSe/ZnS are characterized by optical extinction coefficients ranging from $0.01\,\text{cm}^{-1}$ to $5.9\,\text{cm}^{-1}$. Following available models for QDs in the strong confinement regime [38], it can be found that such values correspond to κ values ranging from 0.01 to 3 [36]. Even higher values $\kappa \sim 4$ have been experimentally retrieved for PbS QDs [39]. Therefore, it can be concluded that it is possible to excite a super-resonant state in coated Si nanospheres with realistic material parameters.

This active configuration also provides new and exciting opportunities in electromagnetic manipulation and microscopy. To illustrate this fact, Fig. 1(b) gives the mechanical force exerted on the particle when it is illuminated by a plane-wave of electric field magnitude $E_0 = 1\,\text{V}/\text{m}$. The force exerted on the particle has been computed by using the analytical formalism introduced in [27, 28], later summarized in this article as Eq. (1). Moreover, since the force is independent of its position for this plane-wave excitation, the particle is centered at the origin of the coordinates for the sake of simplicity. It is apparent from Fig. 1(b) that the mechanical force exerted on the particle is enhanced by several orders of magnitude at its super-resonant state. More strikingly, it can be positive (pushing) or negative (pulling). As suggested in [40, 41], the latter dragging forces correspond to those cases in which the kinetic momentum carried by the incident plane-wave is increased by the stimulated emission being generated by the nanoparticle. Following these studies [40, 41], here we assume a symmetric pumping orthogonal to the direction of propagation (see Fig. 1(b)), so that any force action in the nanoparticle mediated by the pumping can be neglected. However, the aforementioned acceleration and/or dragging effects enhanced by means of stimulated emission entail large scattered fields, possibly resulting in a large and undesired interaction with the environment. In this perspective, the proposed approach of a magnetic dipole super-resonance is advantageous, since the reactive scattered fields excited by the coated Si nanosphere are dominated by the magnetic rather than electric fields, and thus the coupling with the immediate environment is minimized with respect to electric resonances. Moreover, it can be concluded from Fig. 1(b) that the force is totally suppressed at $\kappa \simeq 0.365$. This fact allow us to achieve a high visibility nanoparticle: $Q_{\text{scat}} \simeq 48$ at $\kappa \simeq 0.365$ (see Fig. 2(d)), with a zero-force effect. This configuration could be exploited to develop recoilless optical microscopy techniques. Furthermore, because the electric polarizability itself is not necessary small and is tunable, zero-force effects can be obtained with a certain degree of freedom in the scattering directivity pattern. For example, at the present zero-force configuration ($\kappa = 0.365$), the scattered power is mostly directed against the direction of propagation of the incident field, with a maximum directivity of $D_{\text{scat}} \simeq 2.1$ (see Fig. 2(d)).

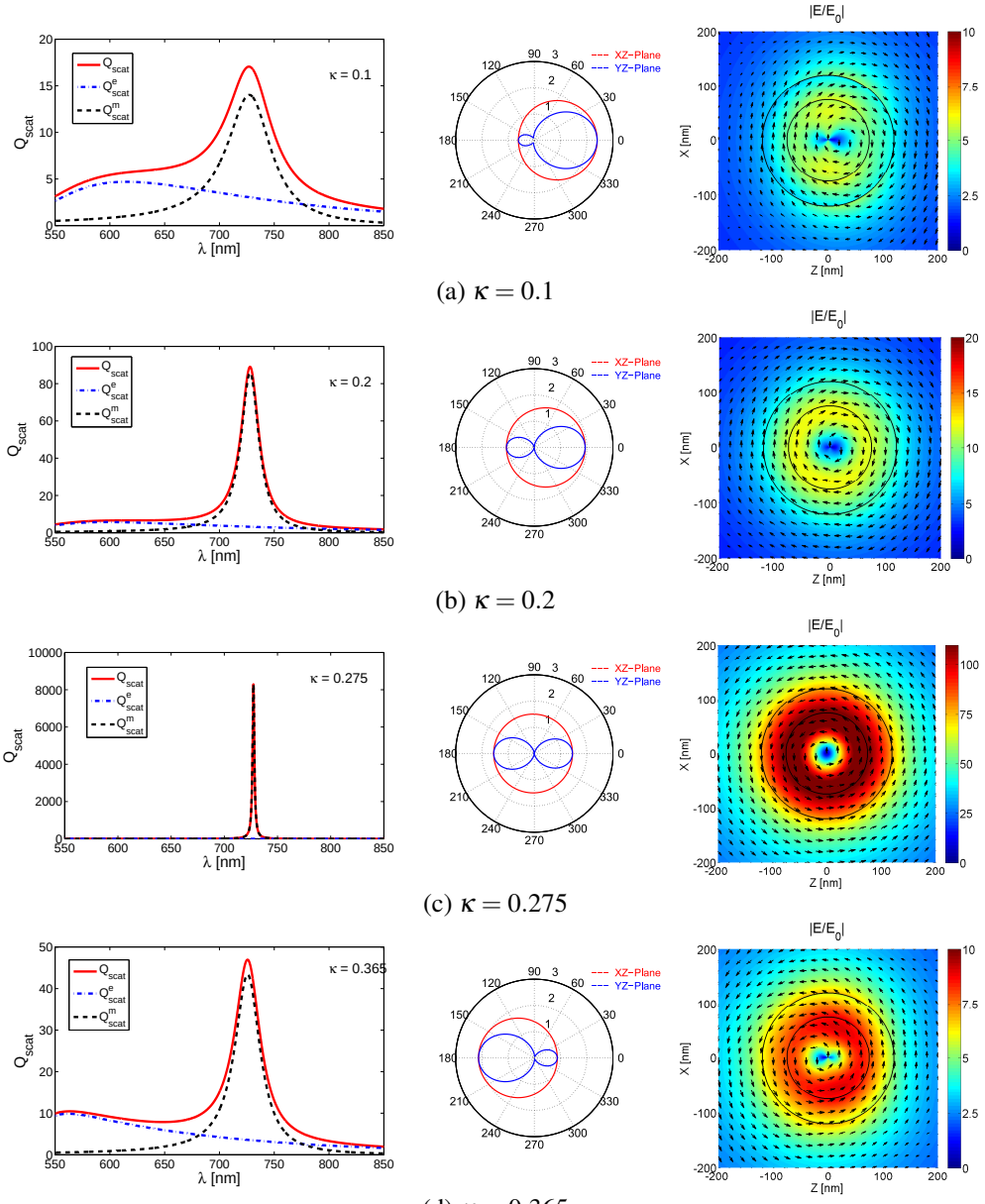

Fig. 2. First column: Scattering efficiency spectrum Q_{scat}, and the contributions to it from the electric and magnetic dipoles, Q^{e}_{scat} and Q^{m}_{scat}. Second column: Scattering directivity patterns, D_{scat}, in the XZ- and YZ-planes. $D_{\text{scat}} = 4\pi r^2 \left(\hat{\mathbf{r}} \cdot \mathbf{S}_{\text{scat}} / P_{\text{scat}}\right)$, where $\mathbf{S}_{\text{scat}} = \frac{1}{2}\text{Re}\left[\mathbf{E}^{\text{scat}} \times \left(\mathbf{H}^{\text{scat}}\right)^{*}\right]$ represents the time-averaged Poynting vector field associated with the scattered field, and $P_{\text{scat}} = \oiint_S \mathbf{S}_{\text{scat}} \cdot \hat{\mathbf{r}}\, dS$ is the time-averaged total scattered power. Third column: Colormap and quiver (arrow) plots of the electric field at the maximum of Q_{scat} . Each row corresponds to a different gain value (a) $\kappa = 0.1$, (d) $\kappa = 0.2$, (c) $\kappa = 0.275$, and (d) $\kappa = 0.365$.

3. Near-field analysis

Next we show that the design flexibility provided by the coated Si nanoparticle enables configurations in which the force exerted on the particle is suppressed, while maintaining a high visibility, even when it is placed in the vicinity of an electromagnetic source (e.g., a probe or a nanoantenna). To this end, note that the time averaged mechanical force exerted on a particle characterized by electric, α_{ee}, and magnetic, α_{mm}, polarizabilities, when it is illuminated with an arbitrary electromagnetic field $(\mathbf{E},\mathbf{H})$, can be written as [27, 28]

$$\mathbf{F}=\frac{1}{2}\mathrm{Re}\left\{\alpha_{ee}\mathbf{E}\cdot(\nabla)\,\mathbf{E}^{*}+\alpha_{mm}\mathbf{H}\cdot(\nabla)\,\mathbf{H}^{*}-\frac{\eta_0 k_0^4}{6\pi\mu_0}\left[\alpha_{ee}\mathbf{E}\times(\alpha_{mm}\mathbf{H})^{*}\right]\right\} \tag{1}$$

In order to compute the force from Eq. (1), the electric and magnetic polarizabilities of the particle can be determined from the Mie theory solution to the scattering problem, as detailed in Appendix A. Moreover, Eq. (1) illustrates how the force exerted on a nanoparticle is a complex function of the electromagnetic field illuminating the particle and its spatial derivatives. Consequently, because of the extreme spatial variations of the fields in the vicinity of a source, obtaining a suppression of the force, not restricted to an specific position, is a cumbersome task. In fact, previous works reporting zero-force effects that apply to near-field scenarios are based either on the compensation of the gradient and absortion/scattering force components [42], or on plasmonic cloaks [43]. However, the former is restricted to very specific spatial points, while the latter implies a vanishing total scattered power. Moreover, both studies are based on particles with negligible magnetic response.

Despite this fact, the symmetry between the contributions to the force associated with the electric and magnetic fields in Eq. (1) suggest that, in theory, it should be possible to suppress the force by opposing those contributions. To achieve this, not only must there be a proper balance between the electric and magnetic responses of the particle, but there also must be a certain degree of symmetry between the electric and magnetic fields illuminating it. In order to construct this equilibrium configuration, it is important to note that, taking advantage of the coated Si nanoparticle, it is possible to find designs in which $\alpha_{ee}=-\alpha_{mm}/\eta_0^2$. This equality applies to both the real and imaginary parts of the polarizabilities, which can only be achieved naturally with an active particle that has a substantial magnetic response, e.g., the proposed active coated Si nanoparticle. Specifically, it has been found that the $\alpha_{ee}=-\alpha_{mm}/\eta_0^2$ condition is satisfied for the particular geometry considered in this article when the active shell has $\kappa=0.568$ at 708 nm.

Moreover, to ensure the symmetry between the electric and magnetic fields illuminating the particle, we propose a canonical source configuration consisting of two aligned electric and magnetic Hertzian dipoles, with current moments $I_e l=I_m l/\eta_0$, respectively, as depicted schematically in Fig. 3(a). For the sake of completeness, explicit expressions of the fields and field-related quantities excited by this source have been included in Appendix A. Due to the dual nature of this source, the electric and magnetic field intensities are proportional, i.e., $|\mathbf{E}|^2=\eta_0^2|\mathbf{H}|^2$, which also implies a zero density of the reactive electromagnetic field energy. Moreover, the dual electric and magnetic dipoles radiate with the same angular, $\sin^2\theta$, power radiation pattern, but with orthogonal polarizations. Furthermore, the densities of the spin angular momentum associated with the electric and magnetic fields are also symmetric. Due to this symmetry, the main force components in Eq. (2) are suppressed. Specifically, introducing closed-form expressions of electric and magnetic Hertzian dipole fields (see, e.g., [44]) into Eq. (1), it is found that the total force exerted on an active and balanced nanoparticle, i.e., when

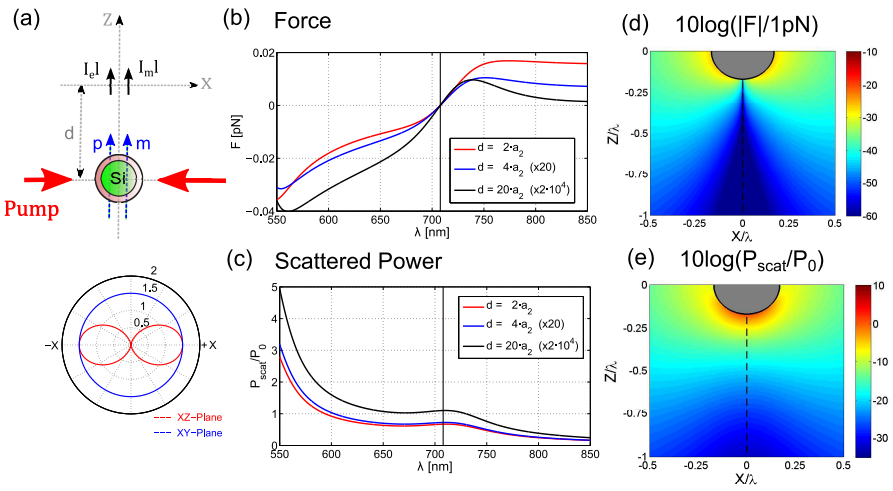

Fig. 3. (a) Sketch of the geometry: Coated Si particle illuminated by two aligned electric and magnetic dipoles with balanced magnitudes $I_e l = I_m l/\eta_0 = 10\,\text{mA}\cdot\text{nm}$. Scattering directivity patterns in the XZ and XY-planes when the nanoparticle is located on the Z-axis. (b) Mechanical force F and (c) scattered power P_{scat} spectra (normalized to the power radiated by the source in free-space P_0) when the nanoparticle is positioned on the $-Z$-axis at the distances $d = 2a_2$, $d = 4a_2$ and $d = 20a_2$ from the source location. Colormaps of the (d) force magnitude and (e) scattered power (in dB scale, normalized, respectively, to 1 pN and P_0) as functions of the particle location on the XZ-plane at $\lambda = 708\,\text{nm}$. The grey areas indicate those locations which are not physically accessible to the nanoparticle.

$\alpha_{ee} = -\alpha_{mm}/\eta_0^2$, is reduced to two residual components given by

$$\mathbf{F} = 2\eta_0^2 k_0^5 \left| \frac{I_e l}{4\pi\,(k_0 r)} \right|^2 \left\{ \hat{\mathbf{r}}\, \frac{2k_0^3}{3\eta_0} \left|\alpha_{ee}\right|^2 \sin\theta - \hat{\phi}\, \alpha''_{ee} \frac{\varepsilon_0}{\omega} \left[\frac{2}{(k_0 r)^2} + \frac{-3}{(k_0 r)^4} \right] \cos\theta \right\} \sin\theta \quad (2)$$

The derivation of Eq. (2) has been included in Appendix A. Since the main force components are cancelled out by the symmetry of the configuration, the residual terms arise from interaction and interference effects between the electric and magnetic dipoles. Specifically, the radial component arises from the interaction between the electric and magnetic dipole fields excited by the particle, while the azimuthal component arises from the force term associated with the density of the spin angular momentum created by the interference between the fields produced by the source electric and magnetic dipoles.

Interestingly, both residual terms vanish along the z-axis ($\theta = 0, \pi$). Therefore, a particle placed along this axis, as schematically depicted on Fig. 3(a), will feel no mechanical force. This effect is evidenced in Fig. 3(b), which illustrates the force exerted on the nanoparticle for different separation distances from the source, $r = d$. It can be concluded from Fig. 3(b) that the force is always zero at $\lambda = 708\,\text{nm}$, no matter what the separation distance from the source is. We believe that this effect can be effectively exploited in particle sorting. For example, small dielectric particles (e.g., those arising as impurities in nano-fabrication processes), are essentially described by an electric polarizability, and therefore are attracted towards the source region due to gradient forces, which are in fact maximized on the z-axis [42]. Therefore, the acceleration exerted by the sources on the coated Si particle, even though it has a much larger scattering cross-section, will be smaller than that of small dielectric particles, allowing to remove those impurities from diluted mixtures of particles with strong magnetic activity.

Moreover, since both the electric *and* magnetic polarizabilities are meaningful, the nanoparticle is scattering a significant amount of power; and, hence, it is visible to external observers. This effect is confirmed by Fig. 3(c), which shows the scattered power spectrum for different distances of separation from the source. This figure also manifests the fact that the particle is not only scattering a significant amount of power, but this occurs at a local maximum. In this configuration and, as illustrated in Fig. 3(a), the electric and magnetic dipoles excited in the nanoparticle are parallel and directed along the z-axis. Consequently, the scattering directivity pattern is characterized by a $\sin^2\theta$ angular variation, no matter what the relative magnitude and phase are between the electric and magnetic dipoles. We believe that this powerful combination of mechanical force suppression and high visibility might trigger innovative paradigms in near-field microscopy.

To further assess these concepts, Figs. 3(d) and 3(e) are, respectively, colormaps of the force magnitude and scattered power as a function of the particle location (center of the particle) on the XZ-plane, at $\lambda = 708\,\text{nm}$. On the one hand, Fig. 3(d) illustrates how the force is suppressed along the z-axis, and how it is weighted by an $\sin\theta$ factor for other locations, as it was predicted by Eq. (2). On the other hand, Fig. 3(e) confirms that the particle scatters a significant amount of power when it is placed along the (zero-force) z-axis. In fact, although there is a null on the source radiation pattern, the reactive fields are maximized along this axis [42]. Consequently, the scattered power is maximized in this axis when the particle is located in the near-field of the sources.

To finalize the discussion, one might wonder what the forces would be in this near field scenario at the magnetic dipole super-resonance (i.e., for κ values closer to the threshold value 0.275). In such a case, the nanoparticle response is dominated by the magnetic dipole resonance, and the force field will be analogous to the force field produced by a localized source acting on a resonant electric dipolar nanoparticle, as studied in [42]. In this manner, the force field will consist of a balance of the gradient, radiation pressure, and curl-spin force components [42], whose magnitudes will all be enhanced by the magnetic dipole super-resonance.

4. Conclusion

In summary, we have demonstrated that it is possible to boost the magnetic dipole resonances present in Si nanoparticles by covering them with a shell impregnated with an active material. This configuration benefits from the concentration of a circulating electric field in the interface between the Si core and the active shell, and thus the magnetic dipole response is several orders of magnitude larger than those excited in bare silicon nanoparticles, and comparable to electric dipole super-resonances excited in spaser-based nanolasers. We believe that such extraordinarily strong magnetic response can be exploited in a wide range of technological applications. Furthermore, this configuration enables a great control on the optical forces exerted on the nanoparticle in both far-field and near-field scenarios. Specifically, colossal pushing and pulling forces are feasible close to the nanoparticle super-resonance. Moreover, it is possible to suppress the force exerted on the nanoparticle even when it is scattering a large amount of power. These effects open up advanced paradigms in electromagnetic manipulation and microscopy. Future efforts might also include the manipulation of the environment surrounding the active nanoparticle. These could include, among others, displacing and rotating the source to control its beam/pattern, optical binding of active/passive nanoparticles to a localized source, and/or compressing the medium in which the nanoparticle is immersed [45].

Appendix A

This appendix provides explicit expressions for the electric and magnetic polarizabilities of a core-shell nanoparticle. To this end, equating the scattered fields predicted by Mie theory to the

fields radiated by equivalent electric and magnetic dipoles, it is possible to derive the following relationships between the $n = 1$ TM and TE scattered field coefficients, and the electric and magnetic polarizabilities of a dipolar particle [46]:

$$\alpha_{ee} = j\frac{6\pi\varepsilon_0}{k_0^3} b_1^{TM}, \quad \alpha_{mm} = j\frac{6\pi\mu_0}{k_0^3} b_1^{TE} \tag{3}$$

The above formulation can be applied to any object, provided that the b_1^{TM} and b_1^{TE} scattered field coefficients are known. For a core-shell structure, these coefficients can be explicitly written as [37]

$$b_1^{TM} = \frac{\eta_s \widehat{J}_1(k_0 a_2)\left[\widehat{J}_1'(k_s a_2) + d_1^{TM}\widehat{H}_1'^{(2)}(k_s a_2)\right] - \eta_0 \widehat{J}_1'(k_0 a_2)\left[\widehat{J}_1(k_s a_2) + d_1^{TM}\widehat{H}_1^{(2)}(k_s a_2)\right]}{\eta_0 \widehat{H}_1'^{(2)}(k_0 a_2)\left[\widehat{J}_1(k_s a_2) + d_1^{TM}\widehat{H}_1^{(2)}(k_s a_2)\right] - \eta_s \widehat{H}_1^{(2)}(k_0 a_2)\left[\widehat{J}_1'(k_s a_2) + d_1^{TM}\widehat{H}_1'^{(2)}(k_s a_2)\right]} \tag{4}$$

with

$$d_1^{TM} = \frac{\eta_c \widehat{J}_1'(k_c a_1)\widehat{J}_1(k_s a_1) - \eta_s \widehat{J}_1(k_c a_1)\widehat{J}_1'(k_s a_1)}{\eta_s \widehat{J}_1(k_c a_1)\widehat{H}_1'^{(2)}(k_s a_1) - \eta_c \widehat{J}_n'(k_c a_1)\widehat{H}_1^{(2)}(k_s a_1)} \tag{5}$$

and

$$b_1^{TE} = \frac{\eta_s \widehat{J'}_1(k_0 a_2)\left[\widehat{J}_1(k_s a_2) + d_1^{TM}\widehat{H}_1^{(2)}(k_s a_2)\right] - \eta_0 \widehat{J}_1(k_0 a_2)\left[\widehat{J'}_1(k_s a_2) + d_1^{TM}\widehat{H}_1'^{(2)}(k_s a_2)\right]}{\eta_0 \widehat{H}_1^{(2)}(k_0 a_2)\left[\widehat{J}_1'(k_s a_2) + d_1^{TM}\widehat{H}_1'^{(2)}(k_s a_2)\right] - \eta_s \widehat{H}_1'^{(2)}(k_0 a_2)\left[\widehat{J}_1(k_s a_2) + d_1^{TM}\widehat{H}_1^{(2)}(k_s a_2)\right]} \tag{6}$$

with

$$d_1^{TE} = \frac{\eta_c \widehat{J}_1(k_c a_1)\widehat{J}_1'(k_s a_1) - \eta_s \widehat{J'}_1(k_c a_1)\widehat{J}_1(k_s a_1)}{\eta_s \widehat{J'}_1(k_c a_1)\widehat{H}_1^{(2)}(k_s a_1) - \eta_c \widehat{J}_n(k_c a_1)\widehat{H}_1'^{(2)}(k_s a_1)} \tag{7}$$

where a_2 and a_1 are, respectively, the external and internal radii of the core-shell structure, which is characterized by the propagation constants k_c and k_s, and medium impedances η_c and η_s, in the core and shell layers, respectively. The terms $\widehat{J}_n(-)$ and $\widehat{H}_n^{(2)}(-)$ are the Schelkunoff forms of the spherical Bessel functions of the first kind and spherical Hankel functions of the second kind, respectively.

To finalize, it is worth remarking that the polarizabilities have been formulated by examining the plane-wave scattering problem [37, 46]. However, since the response of a spherical particle is isotropic, the derived polarizabilities can be applied for arbitrary incident fields.

Appendix B

This appendix includes a detailed analytical description of the fields and field-related quantities excited by a source which is composed of a balanced combination of electric and magnetic Hertzian dipoles oriented along $+\widehat{\mathbf{z}}$, as well as the mechanical forces exerted by such a source on a magnetoelectric particle.

Aligned electric and magnetic Hertzian dipole fields

Consider an electric Hertzian dipole of current moment $I_e l$ located at the origin of the coordinates and oriented along the $+\widehat{\mathbf{z}}$ direction. Assuming that the dipole is driven with a sinusoid at the angular frequency ω, and adopting the $e^{j\omega t}$ time convention, the components of the time-harmonic electromagnetic fields produced by the electric Hertzian dipole: $\mathbf{E}^e = E_r^e\,\widehat{\mathbf{r}} + E_\theta^e\,\widehat{\theta}$,

$\mathbf{H}^e = H_\phi^e\,\widehat{\phi}$, are given by the closed form analytical expressions [44]

$$E_r^e = \frac{\eta_0 k_0^2}{4\pi} I_e l \cdot 2\cos\theta \left[\frac{1}{(k_0 r)^2} + \frac{-j}{(k_0 r)^3}\right] e^{-jk_0 r} \tag{8}$$

$$E_\theta^e = \frac{\eta_0 k_0^2}{4\pi} I_e l \cdot \sin\theta \left[\frac{j}{k_0 r} + \frac{1}{(k_0 r)^2} + \frac{-j}{(k_0 r)^3}\right] e^{-jk_0 r} \tag{9}$$

$$H_\phi^e = \frac{k_0^2}{4\pi} I_e l \cdot \sin\theta \left[\frac{j}{k_0 r} + \frac{1}{(k_0 r)^2}\right] e^{-jk_0 r} \tag{10}$$

where $\eta_0 = \sqrt{\mu_0/\varepsilon_0}$ and $k_0 = \omega\sqrt{\varepsilon_0\mu_0}$ are the impedance and propagation constant, respectively, in free-space. By duality, the fields produced by the magnetic Hertzian dipole of magnetic dipole moment $I_m l = \eta_0 I_e l$, also located at the origin of the coordinates and oriented along $+\widehat{\mathbf{z}}$, can be written as [44]

$$\mathbf{E}^m = \eta_0 \mathbf{H}^e \tag{11}$$

$$\mathbf{H}^m = -\frac{\mathbf{E}^e}{\eta_0} \tag{12}$$

The total electromagnetic field produced by a source composed of these two elementary dipoles is given by the superposition of their fields, i.e.,

$$\mathbf{E} = \mathbf{E}^e + \mathbf{E}^m = \mathbf{E}^e + \eta_0 \mathbf{H}^e \tag{13}$$

$$\mathbf{H} = \mathbf{H}^e + \mathbf{H}^m = \mathbf{H}^e - \frac{\mathbf{E}^e}{\eta_0} \tag{14}$$

Since $\mathbf{E}^e \cdot \mathbf{E}^m = 0$ and $\mathbf{H}^e \cdot \mathbf{H}^m = 0$, the electric and magnetic field intensities can be written as a superposition of the intensities produced by the electric and magnetic Hertzian dipoles alone:

$$|\mathbf{E}|^2 = |\mathbf{E}^e|^2 + |\mathbf{E}^m|^2 = |\mathbf{E}^e|^2 + \eta_0^2 |\mathbf{H}^e|^2 \tag{15}$$

$$|\mathbf{H}|^2 = |\mathbf{H}^e|^2 + |\mathbf{H}^m|^2 = |\mathbf{H}^e|^2 + \frac{|\mathbf{E}^e|^2}{\eta_0^2} \tag{16}$$

It is interesting to notice that the electric and magnetic fields are proportional, with proportionality constant η_0^2, i.e.,

$$|\mathbf{E}|^2 = \eta_0^2 |\mathbf{H}|^2 \tag{17}$$

This balance between the electric and magnetic field intensities also imposes a zero reactive power result, i.e.,

$$P_{\text{reac}} = \frac{\omega}{2} \iiint_V \left(\mu_0 |\mathbf{H}|^2 - \varepsilon_0 |\mathbf{E}|^2\right) dV = 0 \tag{18}$$

In fact, the density of reactive power $\frac{\omega}{2}\left(\mu_0 |\mathbf{H}|^2 - \varepsilon_0 |\mathbf{E}|^2\right)$ is cancelled out identically at all points when this balanced condition is satisfied.

Equation (18) can also be tested by studying the complex Poynting vector field $\mathbf{S} = \mathbf{S}_R + j\mathbf{S}_I = \frac{1}{2}\mathbf{E} \times \mathbf{H}^*$. To this end, note, in virtue of Poynting's theorem, that the reactive power

excited by a localized source can be computed via the flux integral of $\mathbf{S}_I$ through a surface that completely encloses the sources: [44]

$$P_{\text{reac}} = \lim_{\mathbf{r}\to 0} \oiint_S \mathbf{S}_I \cdot \widehat{\mathbf{n}} dS \tag{19}$$

The complex Poynting vector field and its real and imaginary parts are given by the superposition of the corresponding Poynting vector fields associated with the electric and magnetic dipole fields, as well as their cross terms, which represent the interference effects. In particular, one has:

$$\mathbf{S} = \mathbf{S}^e + \mathbf{S}^m + \mathbf{S}^{cross} \tag{20}$$

$$\mathbf{S}_R = \mathbf{S}_R^e + \mathbf{S}_R^m + \mathbf{S}_R^{cross} \tag{21}$$

$$\mathbf{S}_I = \mathbf{S}_I^e + \mathbf{S}_I^m + \mathbf{S}_I^{cross} \tag{22}$$

Since the electric and magnetic dipoles are aligned for our configuration and since they radiate with the same angular power distribution, it can be readily checked that $\mathbf{S}_R^m = \mathbf{S}_R^e$. Moreover, since $\text{Re}\left[\mathbf{A} \times \mathbf{A}^*\right] \equiv 0$, the contribution of the cross product terms to the radiated power is zero: $\mathbf{S}_R^{cross} = 0$. Thus, the total Poynting vector field can be written simply as twice the one associated with the electric Hertzian dipole:

$$\mathbf{S}_R = 2\mathbf{S}_R^e \tag{23}$$

As a consequence, the power radiated into free-space by the combination source, P_0, is simply two times the power radiated by the electric Hertzian dipole or its dual into free-space:

$$P_0 = 2P_0^e = \frac{\eta_0 k_0^2}{6\pi} |I_e l|^2 \tag{24}$$

On the other hand, the symmetry of the fields lead us to $\mathbf{S}_I^m = -\mathbf{S}_I^e$ and $\mathbf{S}_I^{cross} = -2\omega c \mathbf{L}_{SE}^e$ for the imaginary parts of the complex Poynting vector field. This means

$$\mathbf{S}_I = \mathbf{S}_I^{cross} = -2\omega c \mathbf{L}_{SE}^e \tag{25}$$

In other words, the electric and magnetic contributions to $\mathbf{S}_I$ cancel out. The remaining part is due to the cross-terms only; it is proportional to the density of the spin angular momentum of the electric dipole. This implies $\widehat{\mathbf{r}} \cdot \mathbf{S}_I = 0$; and, in view of Eq. (19), this result is consistent with the zero-reactive power property.

Finally, the electric and magnetic densities of the spin angular momentum:

$$\mathbf{L}_{SE} = -\frac{\varepsilon_0}{4j\omega} (\mathbf{E})^* \times \mathbf{E} \tag{26}$$

$$\mathbf{L}_{SH} = -\frac{\mu_0}{4j\omega} (\mathbf{H})^* \times \mathbf{H} \tag{27}$$

can also be subdivided according to the electric dipole, magnetic dipole and interference terms as

$$\mathbf{L}_{SE} = \mathbf{L}_{SE}^e + \mathbf{L}_{SE}^m + \mathbf{L}_{SE}^{cross} \tag{28}$$

$$\mathbf{L}_{SH} = \mathbf{L}_{SH}^e + \mathbf{L}_{SH}^m + \mathbf{L}_{SH}^{cross} \tag{29}$$

Note that since $\mathbf{H}^e$ and $\mathbf{E}^m$ are linearly polarized, their corresponding densities of the spin angular momentum are zero, i.e., $\mathbf{L}_{SE}^m = 0$ and $\mathbf{L}_{SH}^e = 0$. In addition, due to the duality of the sources, it can also be readily checked that

$$\mathbf{L}_{SE}^e = \mathbf{L}_{SM}^m \tag{30}$$

$$\mathbf{L}_{SE}^{cross} = -\mathbf{L}_{SM}^{cross} = \frac{\mathbf{S}_I^e}{\omega c} \tag{31}$$

Mechanical forces exerted on a magnetoelectric particle

According to available analytical techniques, the time-averaged force, $\mathbf{F}$, exerted on a particle that is characterized by electric, α_{ee}, and magnetic, α_{mm}, polarizabilities and is illuminated by an arbitrary electromagnetic field $(\mathbf{E},\mathbf{H})$, can be written as [27, 28]

$$\mathbf{F} = \mathbf{F}_e + \mathbf{F}_m + \mathbf{F}_{e-m} \tag{32}$$

where

$$\mathbf{F}_e = \frac{1}{2}\mathrm{Re}\left\{\alpha_{ee}\mathbf{E}\cdot(\nabla)\,\mathbf{E}^*\right\} = \frac{\alpha'_{ee}}{4}\nabla|\mathbf{E}|^2 + \alpha''_{ee}\left[\eta_0 k_0 \mathbf{S}_R - \frac{\omega}{\varepsilon_0}\nabla\times\mathbf{L}_{SE}\right] \tag{33}$$

$$\mathbf{F}_m = \frac{1}{2}\mathrm{Re}\left\{\alpha_{mm}\mathbf{H}\cdot(\nabla)\,\mathbf{H}^*\right\} = \frac{\alpha'_{mm}}{4}\nabla|\mathbf{H}|^2 + \alpha''_{mm}\left[\frac{k_0}{\eta_0}\mathbf{S}_R - \frac{\omega}{\mu_0}\nabla\times\mathbf{L}_{SH}\right] \tag{34}$$

$$\mathbf{F}_{em} = -\frac{\eta_0 k_0^4}{12\pi\mu_0}\mathrm{Re}\left\{\mathbf{p}\times\mathbf{m}^*\right\} = -\frac{\eta_0 k_0^4}{6\pi\mu_0}\left\{\mathrm{Re}\left[\alpha_{ee}\alpha^*_{mm}\right]\mathbf{S}_R - \mathrm{Im}\left[\alpha_{ee}\alpha^*_{mm}\right]\mathbf{S}_I\right\} \tag{35}$$

Reorganizing these terms, the force can also be written as the combination:

$$\mathbf{F} = \mathbf{F}_{\mathrm{grad}} + \mathbf{F}_{\mathrm{rp}} + \mathbf{F}_{\mathrm{curl}} + \mathbf{F}_{\mathrm{int}} \tag{36}$$

where the gradient, radiation pressure, curl-spin and electric-magnetic interference force components are, respectively, given by [27, 28]

$$\mathbf{F}_{\mathrm{grad}} = \frac{1}{4}\left(\alpha'_{ee}\nabla|\mathbf{E}|^2 + \alpha'_{mm}\nabla|\mathbf{H}|^2\right) \tag{37}$$

$$\mathbf{F}_{\mathrm{rp}} = \eta_0 k_0\left(\alpha''_{ee} + \frac{\alpha''_{mm}}{\eta_0^2} - \frac{k_0^3}{6\pi\mu_0}\mathrm{Re}\left[\alpha_{ee}\alpha^*_{mm}\right]\right)\mathbf{S}_R \tag{38}$$

$$\mathbf{F}_{\mathrm{curl}} = -\omega\left[\frac{\alpha''_{ee}}{\varepsilon_0}\nabla\times\mathbf{L}_{SE} + \frac{\alpha''_{mm}}{\mu_0}\nabla\times\mathbf{L}_{SH}\right] \tag{39}$$

$$\mathbf{F}_{\mathrm{int}} = \frac{\eta_0 k_0^4}{6\pi\mu_0}\mathrm{Im}\left[\alpha_{ee}\alpha^*_{mm}\right]\mathbf{S}_I \tag{40}$$

For our particular choice of a source consisting of two aligned electric and magnetic Hertzian dipoles, these force expressions can be conveniently rewritten as

$$\mathbf{F}_{\mathrm{grad}} = \frac{1}{4}\left(\alpha'_{ee} + \frac{\alpha'_{mm}}{\eta_0^2}\right)\nabla|\mathbf{E}|^2 \tag{41}$$

$$\mathbf{F}_{\mathrm{rp}} = \eta_0 k_0\left(\alpha''_{ee} + \frac{\alpha''_{mm}}{\eta_0^2} - \frac{k_0^3}{6\pi\mu_0}\mathrm{Re}\left[\alpha_{ee}\alpha^*_{mm}\right]\right)\mathbf{S}_R \tag{42}$$

$$\mathbf{F}_{\mathrm{curl}} = -\frac{\omega}{\varepsilon_0}\left[\left(\alpha''_{ee} + \frac{\alpha''_{mm}}{\eta_0^2}\right)\nabla\times\mathbf{L}^e_{SE} + \left(\alpha''_{ee} - \frac{\alpha''_{mm}}{\eta_0^2}\right)\nabla\times\frac{\mathbf{S}^e_I}{\omega c}\right] \tag{43}$$

$$\mathbf{F}_{\mathrm{int}} = -2\omega c\frac{\eta_0 k_0^4}{6\pi\mu_0}\mathrm{Im}\left[\alpha_{ee}\alpha^*_{mm}\right]\mathbf{L}^e_{SE} \tag{44}$$

Explicit expressions of these force components for Hertzian dipole fields can be found by introducing those fields Eqs. (8)-(10) into Eqs. (41)-(44).

This exercise leads to the following relations:

$$\widehat{\mathbf{r}}\cdot\mathbf{F}_{\text{grad}} = -C_{\text{aux}}\left(\alpha'_{ee}+\frac{\alpha'_{mm}}{\eta_0^2}\right)\left[\frac{\sin^2\theta}{(k_0r)^3}+\frac{4\cos^2\theta}{(k_0r)^5}+3\frac{2\cos^2\theta+\sin^2\theta}{(k_0r)^7}\right] \tag{45}$$

$$\widehat{\theta}\cdot\mathbf{F}_{\text{grad}} = C_{\text{aux}}\left(\alpha'_{ee}+\frac{\alpha'_{mm}}{\eta_0^2}\right)\left[\frac{1}{(k_0r)^3}-\frac{2}{(k_0r)^5}-\frac{1}{(k_0r)^7}\right]\sin\theta\cos\theta \tag{46}$$

$$\widehat{\phi}\cdot\mathbf{F}_{\text{grad}} = 0 \tag{47}$$

$$\widehat{\mathbf{r}}\cdot\mathbf{F}_{\text{rp}} = C_{\text{aux}}2\left(\alpha''_{ee}+\frac{\alpha''_{mm}}{\eta_0^2}-\frac{k_0^3}{6\pi\mu_0}\text{Re}\left[\alpha_{ee}\alpha^*_{mm}\right]\right)\frac{\sin^2\theta}{(k_0r)^2} \tag{48}$$

$$\widehat{\theta}\cdot\mathbf{F}_{\text{rp}} = 0 \tag{49}$$

$$\widehat{\phi}\cdot\mathbf{F}_{\text{rp}} = 0 \tag{50}$$

$$\widehat{\mathbf{r}}\cdot\mathbf{F}_{\text{curl}} = C_{\text{aux}}\left(\alpha''_{ee}+\frac{\alpha''_{mm}}{\eta_0^2}\right)\frac{2\cos^2\theta-\sin^2\theta}{(k_0r)^4} \tag{51}$$

$$\widehat{\theta}\cdot\mathbf{F}_{\text{curl}} = C_{\text{aux}}2\left(\alpha''_{ee}+\frac{\alpha''_{mm}}{\eta_0^2}\right)\frac{\sin\theta\cos\theta}{(k_0r)^4} \tag{52}$$

$$\widehat{\phi}\cdot\mathbf{F}_{\text{curl}} = C_{\text{aux}}\left(\alpha''_{ee}-\frac{\alpha''_{mm}}{\eta_0^2}\right)\left\{\frac{2}{(k_0r)^4}+\frac{3}{(k_0r)^6}\right\}\sin\theta\cos\theta \tag{53}$$

$$\widehat{\mathbf{r}}\cdot\mathbf{F}_{\text{int}} = 0 \tag{54}$$

$$\widehat{\phi}\cdot\mathbf{F}_{\text{int}} = C_{\text{aux}}2\frac{k_0^3}{6\pi\mu_0}\text{Im}\left[\alpha_{ee}\alpha^*_{mm}\right]\frac{\sin\theta\cos\theta}{(k_0r)^3} \tag{55}$$

$$\widehat{\theta}\cdot\mathbf{F}_{\text{int}} = 0 \tag{56}$$

where $C_{\text{aux}}\in\mathbb{R}^+$ is an auxiliary constant defined as

$$C_{\text{aux}} = k_0\left|\frac{\eta_0k_0^2}{4\pi}I_el\right|^2 \tag{57}$$

Then the total force on a balanced active particle, i.e., an active particle for which

$$\alpha_{ee} = -\frac{\alpha_{mm}}{\eta_0^2} \tag{58}$$

reduces simply to Eq. (2):

$$\mathbf{F} = \frac{2k_0^4}{3}\left|\alpha_{ee}\right|^2\mathbf{S}_R+2\alpha''_{ee}\nabla\times\frac{\mathbf{S}_I^e}{\omega c}$$
$$= 2\eta_0^2k_0^5\left|\frac{I_el}{4\pi\,(k_0r)}\right|^2\left\{\widehat{\mathbf{r}}\,\frac{2k_0^3}{3\eta_0}\left|\alpha_{ee}\right|^2\sin\theta-\widehat{\phi}\;\alpha''_{ee}\,\frac{\varepsilon_0}{\omega}\left[\frac{2}{(k_0r)^2}+\frac{-3}{(k_0r)^4}\right]\cos\theta\right\}\sin\theta \tag{59}$$

Acknowledgments

This work was supported in part by the Spanish Ministry of Science and Innovation, Projects No. TEC2009-11995 and No. CSD2008-00066 and by the NSF Contract No. ECCS-1126572.